JACS
JOURNAL OF THE AMERICAN CHEMICAL SOCIETY
Article
pubs.acs.org/JACS

Light-Activated Protein Inhibition through Photoinduced Electron Transfer of a Ruthenium(II)–Cobalt(III) Bimetallic Complex

Robert J. Holbrook,[†,‡] David J. Weinberg,[†] Mark D. Peterson,[†] Emily A. Weiss,[†] and Thomas J. Meade*[,†,‡]

[†]Department of Chemistry, Northwestern University, Evanston, Illinois 60208, United States

[‡]Department of Molecular Biosciences, Neurobiology, and Radiology, Northwestern University, Evanston, Illinois 60208, United States

Supporting Information

ABSTRACT: We describe a mechanism of light activation that initiates protein inhibitory action of a biologically inert Co(III) Schiff base (Co(III)-sb) complex. Photoinduced electron transfer (PET) occurs from a Ru(II) bipyridal complex to a covalently attached Co(III) complex and is gated by conformational changes that occur in tens of nanoseconds. Reduction of the Co(III)-sb by PET initiates displacement of the inert axial imidazole ligands, promoting coordination to active site histidines of α-thrombin. Upon exposure to 455 nm light, the rate of ligand exchange with 4-methylimidazole, a histidine mimic, increases by approximately 5-fold, as observed by NMR spectroscopy. Similarly, the rate of α-thrombin inhibition increases over 5-fold upon irradiation. These results convey a strategy for light activation of inorganic therapeutic agents through PET utilizing redox-active metal centers.

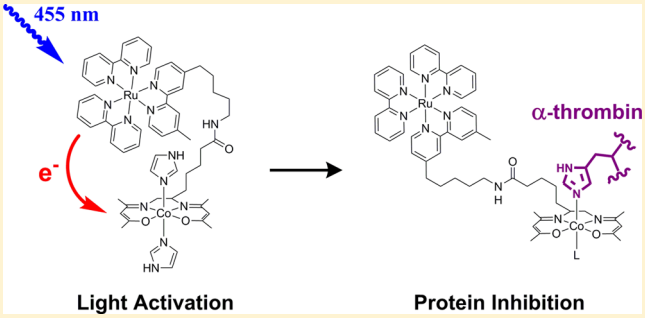

INTRODUCTION

The field of metals in medicine has cultivated the use of coordination complexes in the clinic.[1,2] Since the development of platinum antitumor agents, such as Cisplatin, research has focused on utilizing metal–protein binding interactions to manipulate biological processes and mitigate disease progression. Through exploitation of geometry, coordination number, and redox state of transition metal complexes, metal–protein interactions can be precisely tuned to bind and disrupt the active site of target proteins.[3] In addition, the unique properties of transition metal complexes can be used to facilitate the activation of inert complexes in prodrug strategies.[4−6]

A promising strategy for controlling the spatial and temporal selectivity of a metal-based therapeutic is to activate the prodrug with light.[7,8] The excited state properties of transition metal complexes allow the use of light as an external and orthogonal stimulus to trigger prodrug activation. For example, Turro et al. and Glazer et al. have developed ruthenium photochemotherapeutic agents that undergo photoinduced ligand dissociation to covalently bind DNA and/or release organic chemotherapeutic drugs.[9−12] The excited states of these photochemotherapeutic agents are designed to undergo thermal population from a ^{3}MLCT (metal-to-ligand charge transfer) state to low-lying σ^* ligand field states that promote ligand dissociation.[13] Upon the release of the ligand, the metal center is available to coordinate to DNA. These studies have shown that light can be utilized to exploit the coordination dynamics through the excited state properties of metal-based therapeutics for prodrug strategies.

Cobalt(III) Schiff base (Co(III)-sb) complexes of the equatorial tetradentate ligand bis(acetylacetone)ethylenediimine [acacen] have been extensively studied for their potent protein inhibition activity.[14] Co(III)-sb complexes have been shown to covalently bind active site histidine residues of zinc-dependent proteins through dissociative axial ligand exchange and consequently disrupt protein structure and function.[15] This robust mechanism has enabled inhibition of a wide array of zinc-dependent proteins, including thermolysin, α-thrombin, and matrix metalloproteinase-2.[16−18] Furthermore, selective inhibition of zinc finger transcription factors SP1, Ci, and snail has been achieved through incorporation of biomolecular targeting moieties.[19−22]

The dependency of Co(III)-sb induced protein inhibition on the axial ligands can be utilized for the development of prodrug strategies.[23] Since inhibition activity is dependent on axial ligand exchange, the potency of a Co(III)-sb protein inhibitor can be tuned by selection of the axial ligand.[24,25] Selective enzyme inhibition occurs when the axial coordination sites are occupied by either labile amine or sterically hindered 2-methylimidazole ligands. Conversely, Co(III)-sb complexes with substitutionally inert axial ligands, such as *N*-heterocycles [i.e., imidazole (Im) or 4-methylimidazole (4-MeIm)], are poor

Received: January 12, 2015
Published: February 11, 2015

DOI: 10.1021/jacs.5b00342
J. Am. Chem. Soc. 2015, 137, 3379−3385

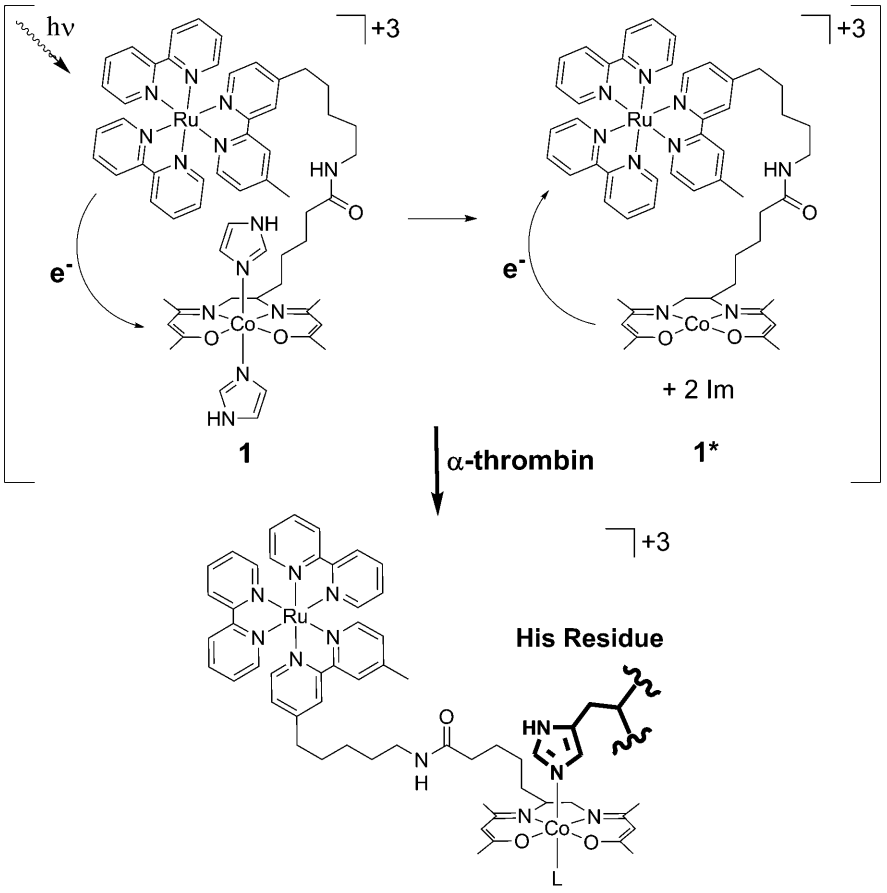

Figure 1. From excitation of Ru(II)-bpy at 455 nm light, the Ru(II)-bpy/Co(III)-sb bimetallic complex undergoes intramolecular PET from a *Ru(II)-bpy ^{3}MLCT state to Co(III)-sb (**1**). PET forms the charge separated Ru(III)-bpy/Co(II)-sb species and promotes axial ligand dissociation (**1***). Oxidation back to Co(III) provides an active Co(III)-sb complex with open axial coordination sites to bind essential histidine residues of α-thrombin (L = Im or His).

protein inhibitors. The axial ligand Im provides an inert protein inhibitor that can be subsequently activated.

Previously, our research has focused on redox activation of the inert Co(III)-sb complex, Co(acacen)$(Im)_2$, through photoinduced electron transfer (PET) from PbS quantum dots (QDs).[23] By irradiation at the energy of the first exitonic absorption of PbS QDs (900 nm), reduction of Co(III)-sb to Co(II)-sb is achieved through PET. Upon reduction to Co(II), axial ligand reactivity increases due to the electron's occupying the antibonding d_{z^2} orbital.[26] Charge recombination back to Co(III) provides the active complex for protein inhibition. Although this mechanism was successful for increasing the axial ligand reactivity of Co(III)-sb with near-infrared light, our particular nanoparticle system was not biocompatible due to the lack of solubility in aqueous solution.

Here, we describe a molecular approach toward the activation of Co(III)-sb protein inhibition using a covalently attached Ru(II) bipyridyl (Ru(II)-bpy) complex to overcome our previous limitations regarding water solubility and biocompatibility (Figure 1). Following photoexcitation of Ru(II)-bpy at 455 nm, this Ru(II)-bpy/Co(III)-sb bimetallic complex undergoes intramolecular PET from the *Ru(II)-bpy ^{3}MLCT state to Co(III)-sb (**1**). The PET process forms the Ru(III)-bpy/Co(II)-sb species and promotes axial ligand dissociation (**1***). The subsequent charge recombination oxidizes the Co(II) metal center back to Co(III) and provides an active Co(III)-sb complex with open axial coordination sites to bind essential histidine residues for protein inhibition (Figure 1). The Ru(II)-bpy/Co(III)-sb system successfully undergoes light-activated inhibition of α-thrombin, an enzyme implicated in the coagulation cascade. Ultimately, this study demonstrates the feasibility of this redox-activated prodrug strategy.

■ RESULTS AND DISCUSSION

The Ru(II)-bpy/Co(III)-sb bimetallic complex (**1**) was synthesized using an amine-functionalized 2,2′-bipyridine and coordinated to the *cis*-bis(bpy)Ru(II) dichloride complex to form **1a**, with a ^{1}MLCT absorption band maximums at 455 nm (see Supporting Information). The pendent bipyridine of Ru(II)-bpy was subsequently peptide coupled to the carboxy-functionalized Co(III)-sb derivative, Co(III)-sb acid, to form complex **1** (Figure 2). Co(III)-sb acid was synthesized and characterized according to literature procedures.[21] The tris-(2,2′-bipyridine)ruthenium(II) [$Ru(bpy)_3$] derivatives were selected for their stability and well characterized oxidative quenching behavior of the ^{3}MLCT state.[27,28] The lowest energy absorption band maximum of Co(III)-sb acid occurs at 410 nm, and the MLCT absorption band structure of **1a** centered around 455 nm is unperturbed by conjugation to Co(III)-sb acid (see the Supporting Information). We conclude that there is only weak coupling of the two metal centers, and irradiation at 455 nm leads to the selective excitation of the Ru(II)-bpy moiety of **1**.

DOI: 10.1021/jacs.5b00342
J. Am. Chem. Soc. 2015, 137, 3379−3385

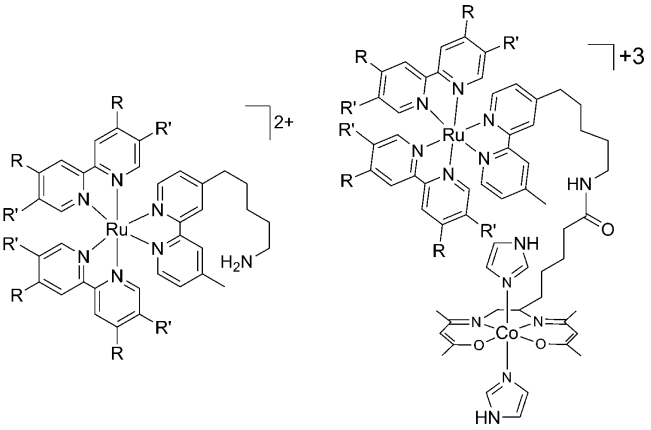

1a; R,R' = -H,-H
2a; R,R' = -Me,-H
3a; R,R' = -Me,-Me

1; R,R' = -H,-H
2; R,R' = -Me,-H
3; R,R' = -Me,-Me

Figure 2. Structure of Ru(II)-bpy/Co(III)-sb bimetallic complexes, **1**, **2**, and **3**, and their respective Ru(II)-bpy precursor, **1a**, **2a**, and **3a**. The pendent bipyridine of each Ru(II)-bpy derivative was subsequently peptide coupled to the carboxy-functionalized Co(III)-sb derivative, Co(III)-sb acid, to form complex **1**, **2**, and **3**.

Activation of the Co(III)-sb complex through reduction requires intramolecular PET from the ^{3}MLCT state of the Ru(II)-bpy complex (populated by photoexcitation and subsequent intersystem crossing) to the Co(III)-sb complex. Subsequent back electron transfer (BET) returns the complex to its ground state (Scheme 1). Based on previously reported reduction potentials of similar $Ru(bpy)_3$ and Co(III)-sb complexes and the $\Delta E_{0,0}$ of the ^{3}MLCT state of **1a**, we estimate, using the Rehm–Weller approximation, that the driving force for the PET reaction for **1** is ~90 meV.[26,29] In the case of **1a** and **1**, the quantum yield of phosphorescence from the parent Ru(II)-bpy complex, **1a**, is reduced by 30% upon covalent conjugation to Co(III)-sb in **1** (from 0.031 to 0.022); see the Supporting Information. These observations are consistent with the presence of an additional decay pathway of the Ru(II)-bpy ^{3}MLCT: namely, PET to Co(III)-sb, in **1**.

In order to determine the time scale of electron transfer between the Ru(II)-bpy and Co(III)-sb moieties of **1**, we measured the transient absorption (TA) spectra of **1a** and **1** in degassed 100 mM phosphate buffer at pH 7.4 at 1.64×10^{-4} M. Figure 3A shows the TA spectrum of **1a** after photoexcitation at 460 nm. The bleach at 460 nm corresponds to depopulation of the **1a** ground state; it recovers via repopulation of the ground state from the ^{3}MLCT state through phosphorescence (process k_o in Scheme 1).[30,31] We found the time constant for decay of the ^{3}MLCT state of **1a** (470 ns) by fitting the kinetic trace at 465 nm (black, Figure 3B) with eq 1:

$$\Delta\mathrm{OD} = \mathrm{IRF}\cdot A_1 e^{-t/\tau_r} \quad (1)$$

where OD is the observed optical density at the wavelength of the ground state bleach ("GSB," 465 nm), IRF is the instrument response function, and A_1 is the amplitude of the relaxation pathway with time constant τ_r.

In the case of the covalently bound Ru–Co complex (**1**), the GSB reflects not only recovery from the ^{3}MLCT state but also the ground state recovery from a convolution of the charge transfer and recombination processes (processes k_{ET} and k_{BET} in Scheme 1).[30,31] The bleach recovery dynamics of **1** are fit by a sum of two simple exponential functions with time constants of 470 ns (A_1 = 0.73) and 38 ns (A_2 = 0.27), convoluted with the IRF, eq 2,

$$\Delta\mathrm{OD} = \mathrm{IRF}\cdot(A_1 e^{-t/\tau_1} + A_2 e^{-t/\tau_2}) \quad (2)$$

when τ_1 is fixed to the time constant for the recovery of the Ru(II)-bpy GSB (470 ns). In order to differentiate the respective influences of the ET and BET processes on the GSB recovery of **1**, we performed time correlated single photon counting (TCSPC) measurements on **1** and **1a**. The Ru(II)-bpy emission dynamics reflect the population of the ^{3}MLCT state and, therefore, are not influenced by charge recombination (k_{BET}).[32] The details of this experimental setup are found in the Supporting Information. Figure 3C shows the TCSPC traces recorded at the emission maximum (615 nm) of **1** and **1a** following photoexcitation at 445 nm. We find that the ^{3}MLCT emission dynamics align closely with the dynamics of the GSB acquired from the TA experiments. The TCSPC trace of **1a** fits to a single exponential decay of 490 ns, while the emission dynamics of **1** fits to eq 2 with time constants of 490 ns (A_1 = 0.50) and 50 ns (A_2 = 0.50).

The agreement between measurements and the fact that only one time constant is required to account for both ET and BET processes, which both must occur in order to fully recover the GSB as observed in Figure 3B, support the following two conclusions: (i) There exists some process which only enables some fraction of the photoexcited Co–Ru complexes in solution to relax via the charge transfer pathway on the tens of nanoseconds time scale, while the remaining fraction decays via phosphorescence. (ii) The 40–50 ns time constant does not correspond to an intrinsic lifetime for ET or BET, but rather for a conformational motion that brings the bimetallic complex into a conformation in which these two processes can occur. We therefore hypothesize that the charge transfer dynamics are the result of conformational gating.[33,34]

In order to verify the role of conformational gating on the observed charge transfer dynamics of **1**, we added two and four methyl groups to the bipyridines of the Ru(II) complex to form Ru(II)-dmb (**2a**) and Ru(II)-tmb (**3a**) (Figure 2). The methyl-functionalized Ru(II) complexes **2a** and **3a** were conjugated to Co(III)-sb acid to form **2** and **3**, which increased the driving force of the PET reaction from ~90 meV to ~240 and ~310 mV, respectively. Based on previous reports of reorganization energies in Ru–Co bimetallic complexes capable of undergoing PET,[35] we estimate that, if the rate constant for GSB recovery corresponds to the rate constant for the elementary PET reaction, this substitution should increase this rate constant by factors of 15 and 50 for **2** and **3**, respectively, relative to that measured for **1**.[36,37] Fits to the dynamics of the GSB to eq 2 for these compounds yield time constants of 300 and 33 ns for **2** and 256 and 28 ns for **3** (Table S1), where, in both fits, the slower time constant is fixed to the phosphorescence decay time constant of the corresponding unattached Ru(II)-bpy (i.e., that of **2a** or **3a**). The small changes in the fast component of the GSB dynamics from that of **1** suggest that the rate of the PET reaction is not dictated by the thermodynamic driving force and therefore is not the rate of the elementary PET reaction.

These findings support our hypothesis that the PET process is conformationally gated such that both PET and BET occur within the lifetime of the donor–acceptor encounter complex. Conformationally gated electron transfer is observed in a variety of donor–acceptor pairs ranging from protein[38] and

DOI: 10.1021/jacs.5b00342
J. Am. Chem. Soc. 2015, 137, 3379–3385

Scheme 1. Energy Level Diagram Showing the Photoinduced Processes of 1[a]

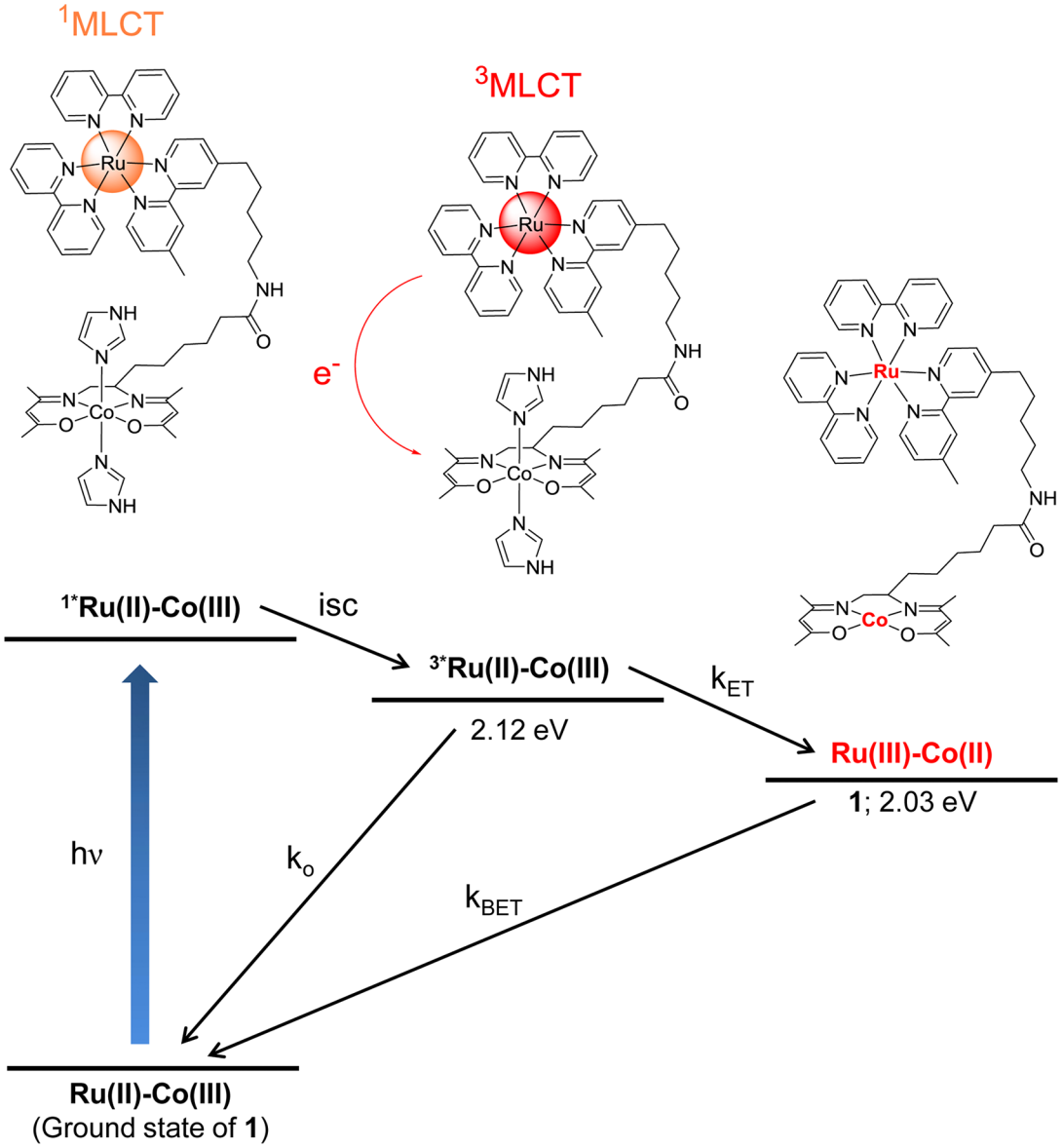

[a]Photoexcitation at 460 nm populates the Ru(II)-bpy ^{1}MLCT state and undergoes intersystem crossing (isc) to the ^{3}MLCT state. Through TA spectroscopy, both the native ^{3}*MLCT excited state decay (k_o) and electron transfer (k_{ET}) to the Co(III)-sb complex is observed for complex **1**. After ET, recovery of the ground state occurs through back electron transfer (k_{BET}) from Co(II)-sb ($k_o = k_r + k_{nr}$, where k_r is phosphorescence and k_{nr} is nonradiative decay).

DNA[39,40] systems to molecular dyads.[41] Typically, donor–acceptor pairs with short alkyl linkers (<3) in which conformational motion gates the PET process will exhibit nanosecond lifetimes for electron transfer,[42,43] while longer linkers, such as polypeptides, have been observed to have gated electron transfer times in the tens of nanoseconds.[44] From these previous studies, we attribute our conformationally gated electron transfer to the flexible alkyl linker between the two metal centers.

Light-Activated Axial Ligand Substitution. In order to determine the effect of PET on Co(III)-sb axial ligand reactivity, we investigated the rate of axial ligand substitution of **1**. Previous studies demonstrate that Co(acacen)$(Im)_2$ in the presence of equal equivalents of 4MeIm results in a mixture of three species: Co(acacen)$(Im)_2$, Co(acacen)(Im)(4MeIm), and Co(acacen)$(4MeIm)_2$ in relative abundances of 25%, 50%, and 25%, respectively. Consequently, the reaction reaches equilibrium with a distribution of 50% Co-Im and 50% Co-4MeIm bonds.[24] Furthermore, PET from PbS QDs was previously observed to increase axial ligand substitution of adsorbed Co(acacen)$(Im)_2$ upon irradiation by 8-fold, relative to the dark control.[23]

The effect of PET on the Co(III)-sb axial ligand reactivity of **1** was determined by monitoring the rate of the ligand exchange reaction in the dark and with irradiation for mixtures of **1**, excess Im, and excess 4MeIm. We added equal equivalents of 4MeIm (8 mM), as the competitive ligand, and Im (8 mM) to a solution of **1** (2.5 mM) in 100 mM phosphate buffer at pH 7.4 and monitored the axial ligand substitution reaction by NMR spectroscopy. In particular, the concentration of Co-Im bonds decrease, while Co-4MeIm bonds increase, to a final equilibrium of 1:1 (Figure 4).

DOI: 10.1021/jacs.5b00342
J. Am. Chem. Soc. 2015, 137, 3379–3385

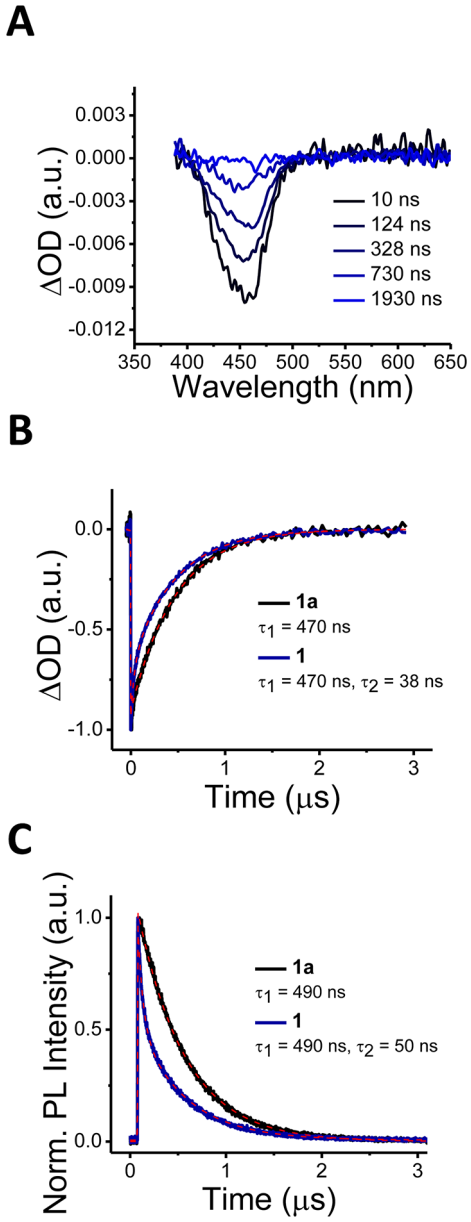

Figure 3. (A) Transient absorption spectra of 1.64×10^{-4} M **1a** in 100 mM phosphate buffer at pH 7.4 in water following photoexcitation at 460 nm. The bleach at 460 nm corresponds to depletion of the Ru(II)-bpy ground state. (B) Kinetic traces extracted from the TA spectrum of the sample of **1a** described in (A), and from the TA spectrum of the covalently bound Co–Ru(II)-bpy complex, **1**, at 465 nm. Red dashed lines correspond to fits of the data as described in the text. (C) Time correlated single photon counting (TCSPC) kinetic traces of Ru(II)-bpy ^{3}MLCT emission of 7.0×10^{-6} M **1** and **1a** in pH 7.4 100 mM phosphate buffer following photoexcitation at 445 nm.

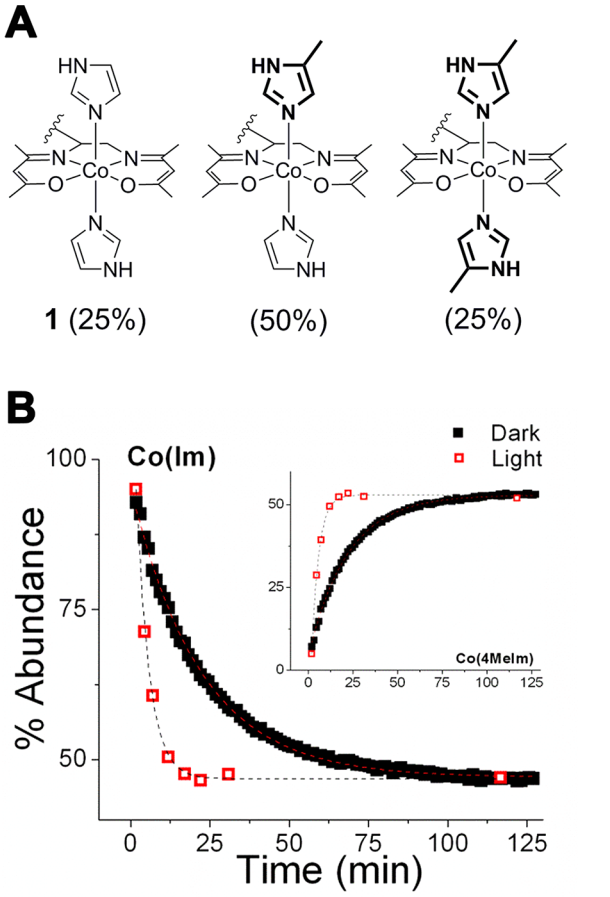

Figure 4. (A) Complex **1** in the presence of equal equivalents of 4MeIm and Im results in a mixture of three species: Ru(II)-bpy/Co(III)-sb(Im)$_2$ (**1**), Ru(II)-bpy/Co(Co(III)-sb(Im)(4MeIm), and Ru(II)-bpy/Co(III)-sb(4MeIm)$_2$ in relative abundances of 25%, 50%, and 25%, respectively. The ligand exchange reaction reaches an equilibrium distribution of 50% Co-Im bonds and 50% Co-4MeIm bonds. (B) Abundance of imidazole bound to Co ("Co(Im)") and 4MeIm bound to Co "Co(4MeIm)" (inset) within mixtures of 2.5 mM **1**, 8 mM Im, and 8 mM 4MeIm, where the reaction was monitored by NMR in the dark (black solid) and under illumination (red open) with three 4-W LED lights (λ_{irr} = 455 nm). Intramolecular PET from the photoexcited Ru(II)-bpy of **1** decreases the time constant for axial ligand substitution from 22 to 4 min.

Photoactivation of **1** was performed by illuminating the sample in an NMR tube with three 4-W LED lights that emit 455 nm light. The NMR spectrum of the reaction mixture was acquired immediately following illumination for a single time point. This method was repeated for each time point for 0, 5, 10, 15, 20, 25, and 30 min. With exposure to light, the final equilibrium state of the axial ligand substitution reaction is completed with a time constant of 4 min (Figure 4, red open squares). This time constant was compared to that for **1** with equal equivalents of Im and 4MeIm, prepared under identical conditions to the first sample, but monitored in the dark. For the dark control, the final equilibrium state for the axial ligand substitution reaction is completed with a time constant of 22 min (Figure 4, black solid squares). This study demonstrates that intramolecular PET from the Ru(II)-bpy to the Co(III)-sb increases the rate of the axial ligand substitution of **1** with 4MeIm by a factor of 5.5.

Light-Activated Inhibition of α-Thrombin. To investigate the use of **1** for light-activated protein inhibition, we performed enzyme inhibition assays on human α-thrombin. Thrombin is a serine protease that has been implicated in the blood coagulation cascade as it converts fibrinogen into fibrin, which ultimately cross-links to form blood clots.[45] Due to its role in blood coagulation, inhibition of thrombin may help prevent the reocclusion of coronary arteries after thrombolytic therapy following a myocardial infarction.[46] Previously, we have found Co(III)-sb complexes are potent irreversible inhibitors of human α-thrombin activity via an axial ligand exchange

DOI: 10.1021/jacs.5b00342
J. Am. Chem. Soc. 2015, 137, 3379–3385

mechanism and provides an established enzyme system for investigating light-activated strategies.[16,17]

We prepared a stock solution of 100 μM of **1** with 4.0 units/mL of human α-thrombin in 100 mM TRIS and 10 mM sodium azide buffer at pH 7.4. The enzyme activity of α-thrombin was monitored over time by diluting a 15 μL aliquot of the stock solution for each time point to 1 mL of run buffer (100 mM TRIS buffer at pH 7.4) and measuring the rate of enzyme-catalyzed hydrolysis of 200 μM of the chromogenic substrate, Sar-Pro-Arg-pNA (see Supporting Information). The stock solution was kept either in the dark or under irradiation with 455 nm light. Aliquots were taken from this stock to assay the enzyme activity over time and evaluate the rate of inhibition of α-thrombin by **1** (Figure 5). Under dark conditions, the

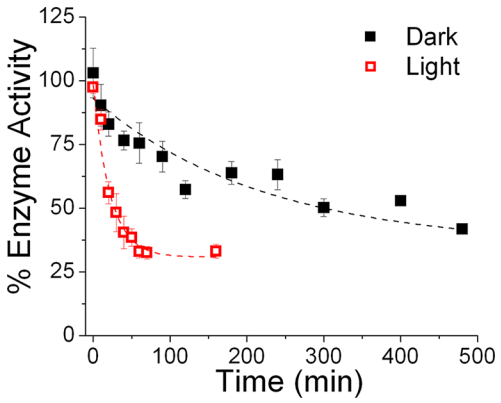

Figure 5. Inhibition of α-thrombin (4.0 units/mL) by **1** (100 μM) in 100 mM TRIS and 10 mM sodium azide buffer at pH 7.4 was monitored over time by enzyme activity in the dark (black) and under illumination (red) with a 4-W LED light (λ_{irr} = 455 nm). Enzyme assays to determine enzyme activity were done in triplicate, and SEMs are shown. Intramolecular PET from the photoexcited Ru(II)-bpy of **1** increases the k_{app} of enzyme inhibition of α-thrombin from 6.8×10^{-5} to 3.8×10^{-4} s^{-1}.

pseudo-first-order rate constant (k_{app}) for enzyme inhibition was found to be 6.8×10^{-5} s^{-1}. Upon irradiation with 455 nm light, the k_{app} for enzyme inhibition was increased to 3.8×10^{-4} s^{-1}.

These studies demonstrate that intramolecular PET from Ru(II)-bpy to the Co(III)-SB of **1** increases the rate of enzyme inhibition of α-thrombin by a factor of 5.6 under these conditions. Complex **1** is a water-soluble, biocompatible prodrug that utilizes a new mechanism for light-activated protein inhibition.

CONCLUSION

We have shown that selective photoexcitation of Ru(II)-bpy of **1** increases the axial ligand reactivity of Co(III)-sb. The rate of axial ligand substitution of Im with 4MeIm, a His mimic, occurs more than five times faster relative to dark conditions. Through PET, axial ligand reactivity of Co(III)-sb can be controlled using light. Similarly, photoexcitation of **1** increases the rate of inhibition of α-thrombin relative to dark conditions by a factor of 5.6. We propose that the mechanism is intramolecular electron transfer from Ru(II)-bpy to Co(III)-sb, given that (i) previous studies have shown the displacement of the axial ligands is a consequence of reduction of Co(III) to Co(II) through a PET process for this family of Co(III)-sb complexes,[23,26] (ii) electron transfer from the ^{3}MLCT state of Ru(II)-bpy to Co(III) is energetically favorable by ~90 meV, while energy transfer is not thermodynamically possible, and (iii) the presence of both Ru(II) and Co(III) is required for electron transfer to occur, while the bimolecular electron transfer between $Ru(bpy)_3$ and $Co(acacen)(Im)_2$ was not observed in similar conditions.

The conformationally gated electron transfer observed for **1**−**3** is attributed to the flexible alkyl linker between the two metal centers. These studies show further structural development is required to increase the efficiency of the electron transfer process for light activation. Due to the similarity in the electron transfer kinetics, **1** was selected for further evaluation as a light-activated protein inhibitor. We investigated the effect of irradiation on the axial ligand substitution of Co(III)-sb through NMR spectroscopy, similar to our previously studied QD system.[23] The time constant for axial ligand exchange of **1** with the histidine mimic, 4MeIm, of 4 min is a 30% improvement from the QD system with a rate of 5.5 min. Although these systems utilize different photosensitizers, the similarity in enhancement of axial ligand exchange upon irradiation shows the versatility of this light-activated strategy—as long as the thermodynamic requirements for PET are met, redox activation of the Co metal center increases the axial ligand reactivity. Furthermore, the water solubility of **1** allows the evaluation for light-activated protein inhibition. Our measured enhancement of k_{app} for enzyme inhibition of α-thrombin by **1** from 6.8×10^{-5} to 3.8×10^{-4} s^{-1} shows the increase in axial ligand reactivity upon irradiation facilitates an increase in the rate of protein inhibition.

Our results offer a new method for light activation of a bimetallic Ru(II)−Co(III)-sb protein inhibitor via 455 nm excitation and provide a platform for the development of inorganic therapeutic agents that can be activated by cooperative redox-binding ligation. Our studies show that mechanisms of the described phenomena are applicable in biologically relevant conditions and provide the light activation of protein inhibition. Furthermore, we show synthetic attachment of Ru(II)-bpy and Co(III)-sb is required for PET to occur. Additionally, our studies reveal that thermodynamics of the PET reaction is limited by the conformation of the bimetallic construct. In order to increase the efficiency of the PET reaction and improve subsequent activation, structural modification between the donor−acceptor pair will be required. Future work will focus on refining the system to enhance the efficiency of the electron transfer process through modification of the linker and supramolecular constructs.

ASSOCIATED CONTENT

Supporting Information

Experimental details and additional electron transfer-related calculations. This material is available free of charge via the Internet at http://pubs.acs.org.

AUTHOR INFORMATION

Corresponding Author

*tmeade@northwestern.edu

Notes

The authors declare no competing financial interest.

ACKNOWLEDGMENTS

This work was supported by the David and Lucile Packard Foundation through a Packard Foundation Fellowship for

DOI: 10.1021/jacs.5b00342
J. Am. Chem. Soc. 2015, 137, 3379−3385

Science and Engineering to E.A.W., the National Institutes of Health's Centers of Cancer Nanotechnology Excellence initiative of the National Cancer Institute under Award U54CA151880, the National Cancer Institute under Award R03CA167715, the National Institutes of Health-National Institute of Arthritis and Musculoskeletal and Skin Diseases under Award P30AR057216, and the Rosenberg Cancer Foundation. D.J.W. is funded by the Department of Energy Office of Science Graduate fellowship program (DOE SCGF), which is administered by ORISE-ORAU under Contract Number DE-AC05-06OR23100. Metal analysis was performed at the Northwestern University Quantitative Bioelemental Imaging Center generously supported by NASA Ames Research Center Grant NNA04CC36G.

REFERENCES

(1) Mjos, K. D.; Orvig, C. *Chem. Rev.* **2014**, *114*, 4540.
(2) Barry, N. P. E.; Sadler, P. J. *Pure Appl. Chem.* **2014**, *86*, 1897.
(3) Hambley, T. W. *Science* **2007**, *318*, 1392.
(4) Farrer, N. J.; Salassa, L.; Sadler, P. J. *Dalton Trans.* **2009**, 10690.
(5) Graf, N.; Lippard, S. J. *Adv. Drug Delivery Rev.* **2012**, *64*, 993.
(6) Zhang, J. Z.; Bonnitcha, P.; Wexselblatt, E.; Klein, A. V.; Najajreh, Y.; Gibson, D.; Hambley, T. W. *Chem.—Eur. J.* **2013**, *19*, 1672.
(7) Smith, N. A.; Sadler, P. J. *Philos. Trans. R. Soc. London, Ser. A* **2013**, *371*, 20120519.
(8) Pizarro, A. M.; McQuitty, R. J.; Mackay, F. S.; Zhao, Y.; Woods, J. A.; Sadler, P. J. *ChemMedChem* **2014**, *9*, 1169.
(9) Garner, R. N.; Gallucci, J. C.; Dunbar, K. R.; Turro, C. *Inorg. Chem.* **2011**, *50*, 9213.
(10) Heidary, D. K.; Howerton, B. S.; Glazer, E. C. *J. Med. Chem.* **2014**, *57*, 8936.
(11) Howerton, B. S.; Heidary, D. K.; Glazer, E. C. *J. Am. Chem. Soc.* **2012**, *134*, 8324.
(12) Knoll, J. D.; Turro, C. *Coord. Chem. Rev.* **2015**, *282*−*283*, 110.
(13) Garner, R. N.; Joyce, L. E.; Turro, C. *Inorg. Chem.* **2011**, *50*, 4384.
(14) Heffern, M. C.; Yamamoto, N.; Holbrook, R. J.; Eckermann, A. L.; Meade, T. J. *Curr. Opin. Chem. Biol.* **2013**, *17*, 189.
(15) Heffern, M. C.; Kurutz, J. W.; Meade, T. J. *Chem.—Eur. J.* **2013**, *19*, 17043.
(16) Takeuchi, T.; Bottcher, A.; Quezada, C. M.; Meade, T. J.; Gray, H. B. *Bioorg. Med. Chem.* **1999**, *7*, 815.
(17) Takeuchi, T.; Böttcher, A.; Quezada, C. M.; Simon, M. I.; Meade, T. J.; Gray, H. B. *J. Am. Chem. Soc.* **1998**, *120*, 8555.
(18) Harney, A.; Sole, L.; Meade, T. *J. Biol. Inorg. Chem.* **2012**, *17*, 853.
(19) Harney, A. S.; Lee, J.; Manus, L. M.; Wang, P.; Ballweg, D. M.; LaBonne, C.; Meade, T. J. *Proc. Natl. Acad. Sci. U.S.A.* **2009**, *106*, 13667.
(20) Harney, A. S.; Meade, T. J.; LaBonne, C. *PLoS One* **2012**, *7*, e32318.
(21) Hurtado, R. R.; Harney, A. S.; Heffern, M. C.; Holbrook, R. J.; Holmgren, R. A.; Meade, T. J. *Mol. Pharmaceutics* **2012**, *9*, 325.
(22) Böttcher, A.; Gray, H. B.; Meade, T. J.; Simon, M. I.; Takeuchi, T. *J. Inorg. Biochem.* **1995**, *59*, 221.
(23) Peterson, M. D.; Holbrook, R. J.; Meade, T. J.; Weiss, E. A. *J. Am. Chem. Soc.* **2013**, *135*, 13162.
(24) Manus, L. M.; Holbrook, R. J.; Atesin, T. A.; Heffern, M. C.; Harney, A. S.; Eckermann, A. L.; Meade, T. J. *Inorg. Chem.* **2013**, *52*, 1069.
(25) Matosziuk, L. M.; Holbrook, R. J.; Manus, L. M.; Heffern, M. C.; Ratner, M. A.; Meade, T. J. *Dalton Trans.* **2013**, *42*, 4002.
(26) Böttcher, A.; Takeuchi, T.; Hardcastle, K. I.; Meade, T. J.; Gray, H. B.; Cwikel, D.; Kapon, M.; Dori, Z. *Inorg. Chem.* **1997**, *36*, 2498.
(27) Balzani, V.; Juris, A. *Coord. Chem. Rev.* **2001**, *211*, 97.
(28) Brown, A. M.; McCusker, C. E.; McCusker, J. K. *Dalton Trans.* **2014**, *43*, 17635.
(29) Elliott, C. M.; Freitag, R. A.; Blaney, D. D. *J. Am. Chem. Soc.* **1985**, *107*, 4647.
(30) Abrahamsson, M. L. A.; Baudin, H. B.; Tran, A.; Philouze, C.; Berg, K. E.; Raymond-Johansson, M. K.; Sun, L.; Åkermark, B.; Styring, S.; Hammarström, L. *Inorg. Chem.* **2002**, *41*, 1534.
(31) Berglund-Baudin, H.; Sun, L.; Davidov, R.; Sundahl, M.; Styring, S.; Åkermark, B.; Almgren, M.; Hammarström, L. *J. Phys. Chem. A* **1998**, *102*, 2512.
(32) Opperman, K. A.; Mecklenburg, S. L.; Meyer, T. J. *Inorg. Chem.* **1994**, *33*, 5295.
(33) Hoffman, B. M.; Ratner, M. A. *J. Am. Chem. Soc.* **1987**, *109*, 6237.
(34) Gray, H. B.; Winkler, J. R. *Biochim. Biophys. Acta, Bioenerg.* **2010**, *1797*, 1563.
(35) Yoshimura, A.; Nozaki, K.; Ikeda, N.; Ohno, T. *J. Am. Chem. Soc.* **1993**, *115*, 7521.
(36) Seidel, R.; Faubel, M.; Winter, B.; Blumberger, J. *J. Am. Chem. Soc.* **2009**, *131*, 16127.
(37) Solis, B. H.; Hammes-Schiffer, S. *Inorg. Chem.* **2011**, *50*, 11252.
(38) Winkler, J. R.; Gray, H. B. *Chem. Rev.* **1992**, *92*, 369.
(39) Prunkl, C.; Berndl, S.; Wanninger, W.; Barbaric, J.; Wagenknecht, H.-A. *Phys. Chem. Chem. Phys.* **2010**, *12*, 32.
(40) Valis, L.; Wang, Q.; Raytchev, M.; Buchvarov, I.; Wagenknecht, H.-A.; Fiebig, T. *Proc. Natl. Acad. Sci. U.S.A.* **2006**, *103*, 10192.
(41) Benniston, A. C.; Harriman, A. *Chem. Soc. Rev.* **2006**, *35*, 169.
(42) Tkachenko, N. V.; Tauber, A. Y.; Grandell, D.; Hynninen, P. H.; Lemmetyinen, H. *J. Phys. Chem. A* **1999**, *103*, 3646.
(43) Batteas, J. D.; Harriman, A.; Kanda, Y.; Mataga, N.; Nowak, A. K. *J. Am. Chem. Soc.* **1990**, *112*, 126.
(44) Jones, G., II; Zhou, X.; Vullev, V. I. *Photochem. Photobiol. Sci.* **2003**, *2*, 1080.
(45) Coughlin, S. R. *J. Thromb. Haemostasis* **2005**, *3*, 1800.
(46) Fitzgerald, D. J.; Fitzgerald, G. A. *Proc. Natl. Acad. Sci. U.S.A.* **1989**, *86*, 7585.

DOI: 10.1021/jacs.5b00342
J. Am. Chem. Soc. 2015, 137, 3379−3385